Supplementary

Table S1 Parameters of different MRI scanners

MRI scanners	Sources	Number of patients scanned
Magnetom Aera 1.5T imager	Siemens Healthcare, Erlangen, Germany	53
3.0T UIHMR770 scanner	United Imaging Healthcare, Shanghai, China	92
Magnetom Avanto 1.5T imager	Siemens Healthcare, Erlangen, Germany	40
1.5T UIHMR560 scanner	United Imaging Healthcare, Shanghai, China	74
Magnetom Verio 3.0T MRI System	Siemens Healthcare, Erlangen, Germany	12
Prisma 3.0T MRI System	Siemens Healthcare, Erlangen, Germany	24
Ingenia CX3.0 MRI System	Philips Medical Systems, Best, Netherlands	25

Table S2 Gd-DTPA MR imaging sequences and parameters

Parameter	T2WI-FS	DWI	IP-OP T1WI	3D-VIBE T1WI
Repetition time (msec)	3500	3200	230	4.38
Echo time (msec)	84	56	2.38 and 4.76	1.93
Slice thickness (mm)	5.5	5.5	5.5	3-4
Matrix size	320×224	128×128	320×240	320×240
Field of view (mm^2)	380×308	380×308	380×278	380×297
Gap (mm)	1.1	1.1	1.1	0
Average	1	1	1	1

Table S3 The numbers of the selected features of each sequences during the procedure of feature selection

Model name	Input features	Feature numbers (N)		
		Mann-Whitney U test (P<0.05)	Spearman's rank correlation coefficient (P>0.9)	LASSO selection
AP	1197	169	39	7
PVP	1197	164	46	13
DP	1197	160	34	9
Combined	3591	489	109	10

https://dx.doi.org/10.21037/jgo-2025-1-1026

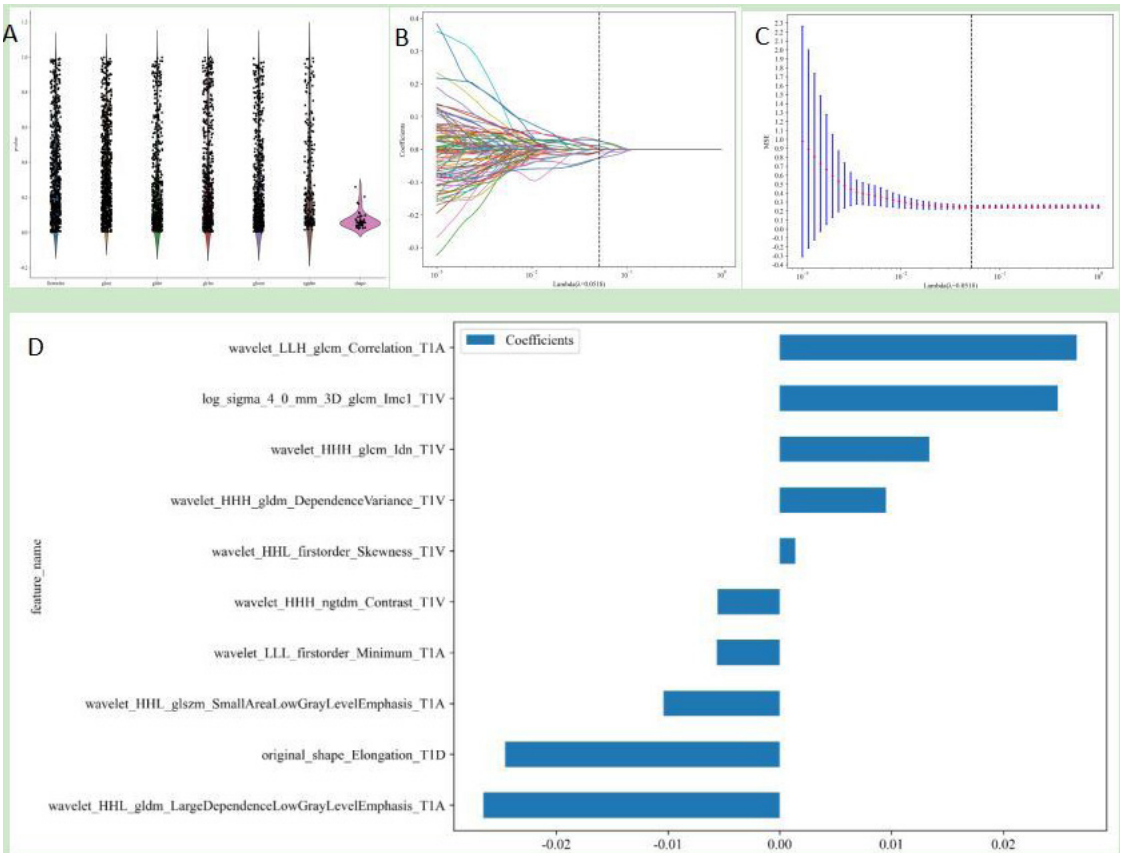

Figure S1 The distribution plot of retained radiomics signatures (A). Using the LASSO method with tenfold cross-validation based on the minimum binomial deviation, the most valuable signatures with nonzero coefficients were identified (B). At lambda (λ) =0.0518 (C). The weighted importance of the selected ten signatures (D).

https://dx.doi.org/10.21037/jgo-2025-1-1026

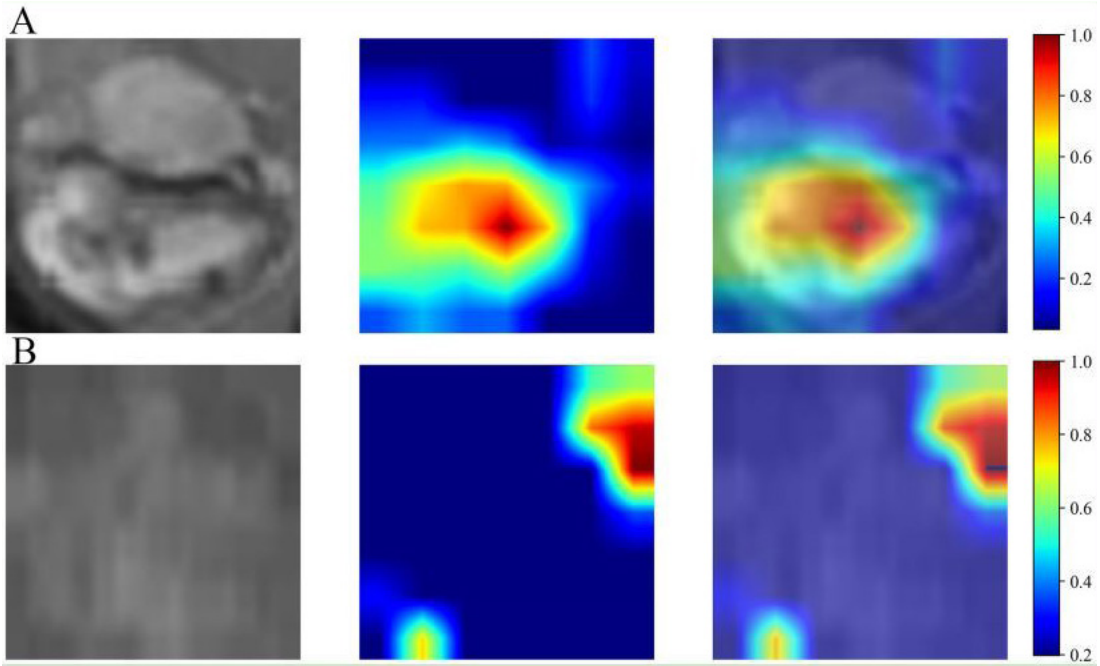

Figure S2 Attention heatmap drawn by class activation mapping. Darker red indicates greater contribution for P53 prediction, while darker blue indicates lower contribution. (A) Case of a 69-year-old man with pathologically confirmed HCC with P53 mutation; (B) Case of a 72-year-old man with pathologically confirmed HCC without P53 mutation.

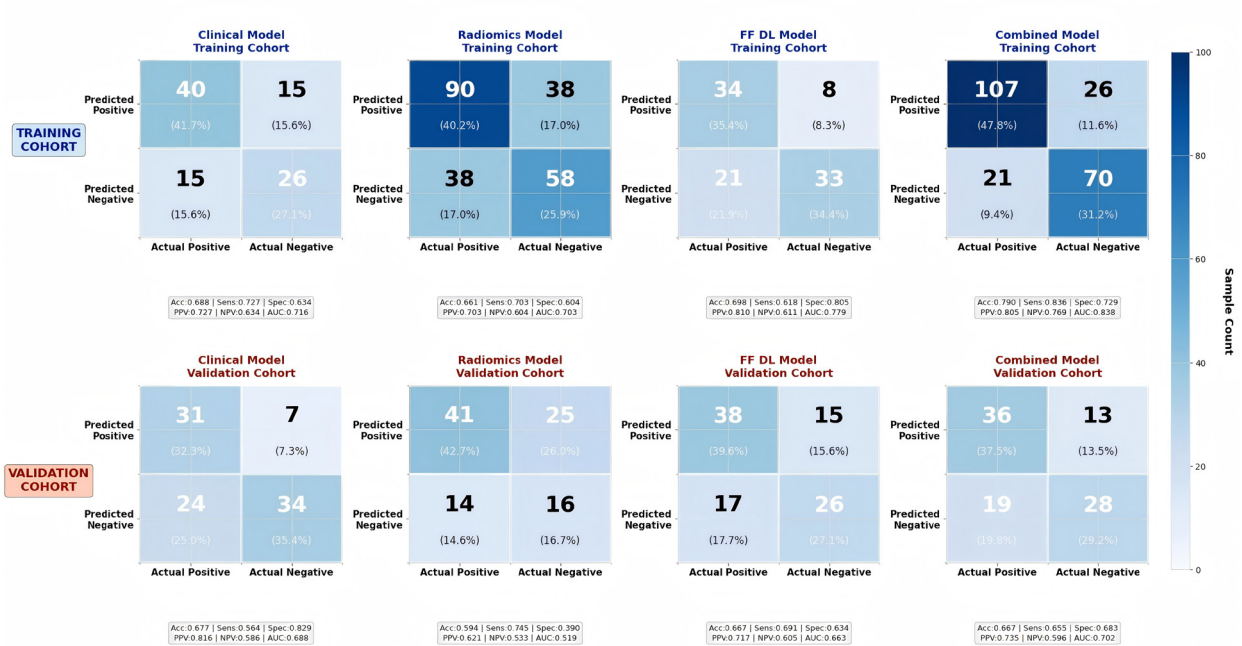

Figure S3 Confusion matrices of the clinical, radiomics, FF DL, and combined models in the training and validation cohorts. The heatmaps display the number and percentage of correctly and incorrectly classified cases for each model. Performance metrics including accuracy (Acc), sensitivity (Sens), specificity (Spec), positive predictive value (PPV), negative predictive value (NPV), and area under the curve (AUC) are provided below each matrix.

https://dx.doi.org/10.21037/jgo-2025-1-1026

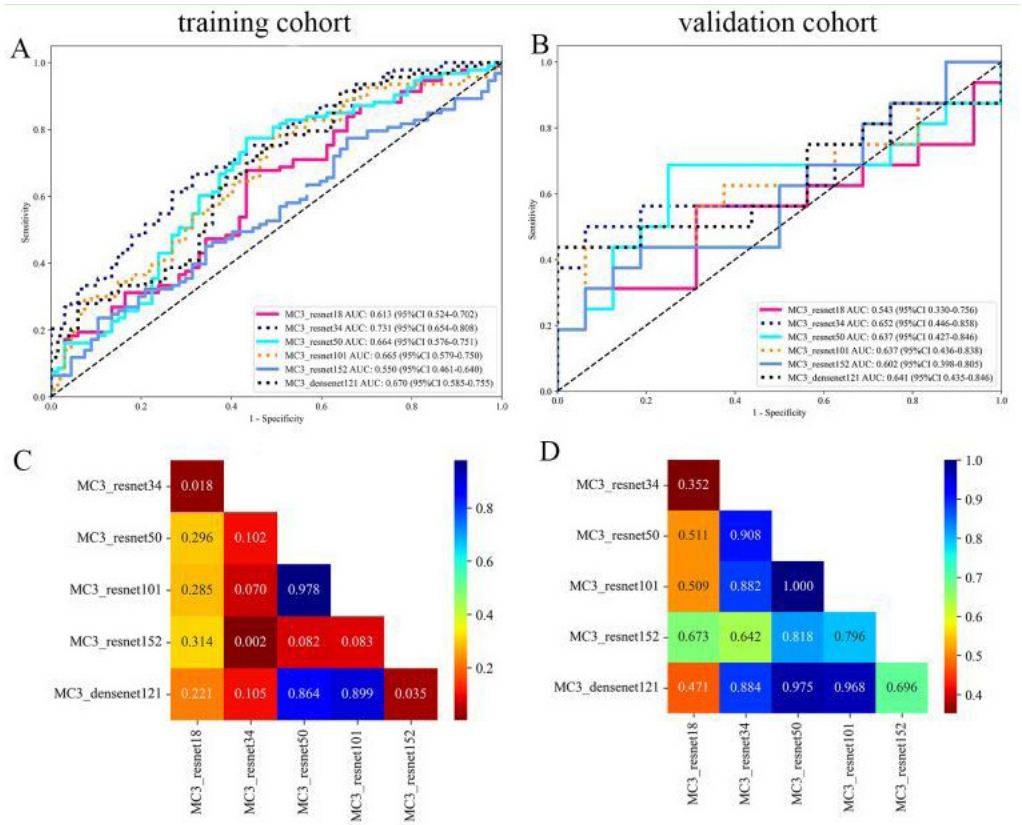

Figure S4 Presents the ROC curves (A: training cohort, B: validation cohort) and DeLong tests (C: training cohort, D: validation cohort) for the assessment of the MC DL prediction model. These visual and statistical analyses provide a comprehensive evaluation of the model's predictive capabilities across various CNNs.

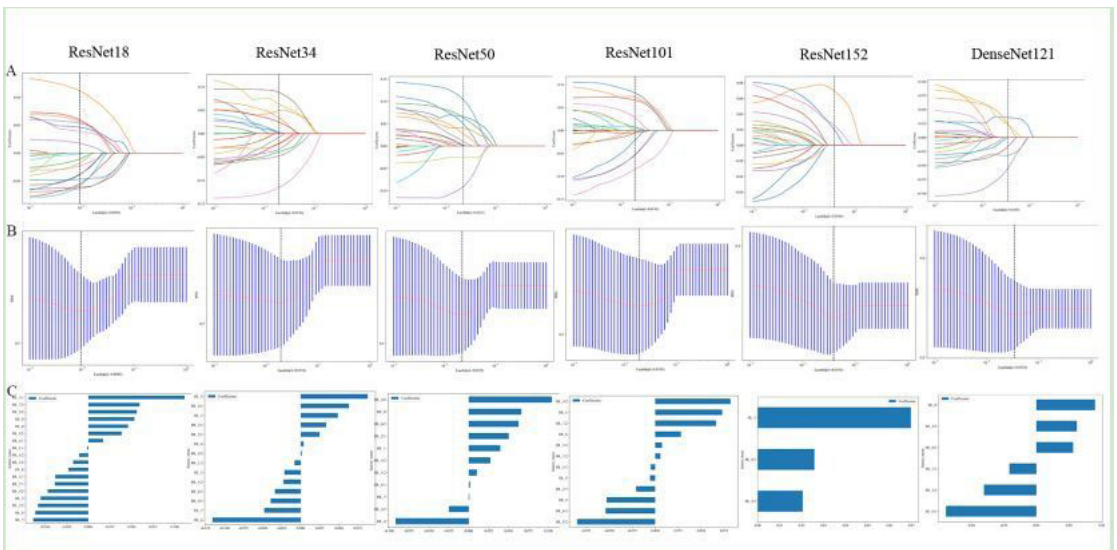

Figure S5 Filtering the features of 6 CNNs from the FF DL model. (A) LASSO regression coefficient of the features. Different color line shows corresponding coefficient of each feature; (B) Tuning parameter (λ) selection in LASSO model; C. Values of fusion features.

https://dx.doi.org/10.21037/jgo-2025-1-1026

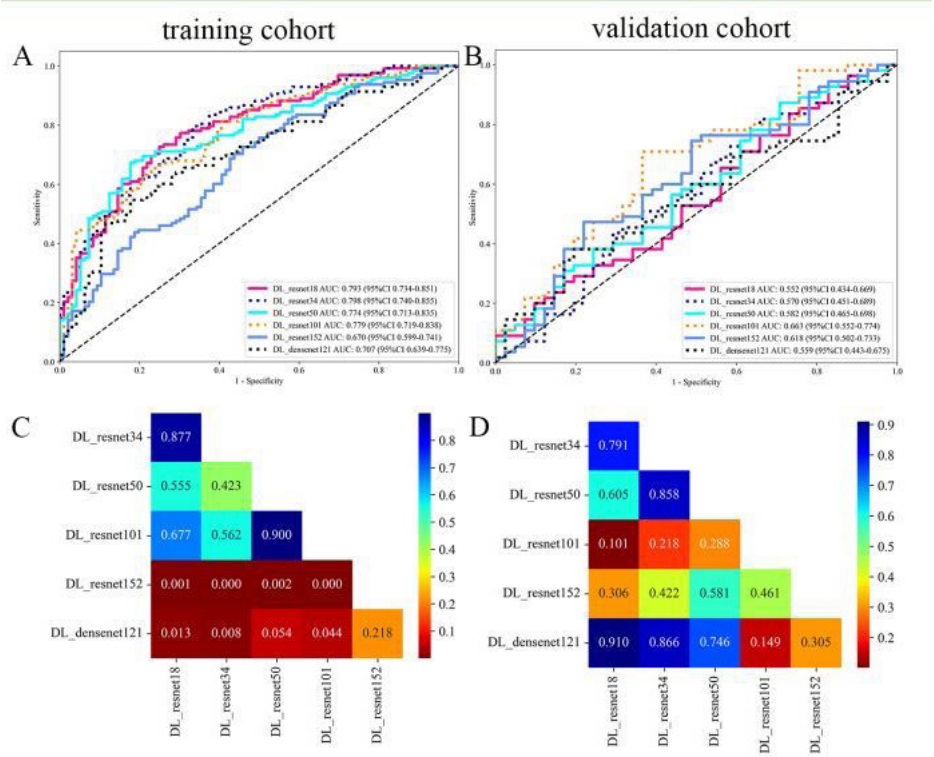

Figure S6 Presents the ROC curves (A: training cohort, B: validation cohort) and DeLong tests (C: training cohort, D: validation cohort) for the assessment of the FF DL prediction model. These visual and statistical analyses provide a comprehensive evaluation of the model's predictive capabilities across various CNNs.

https://dx.doi.org/10.21037/jgo-2025-1-1026

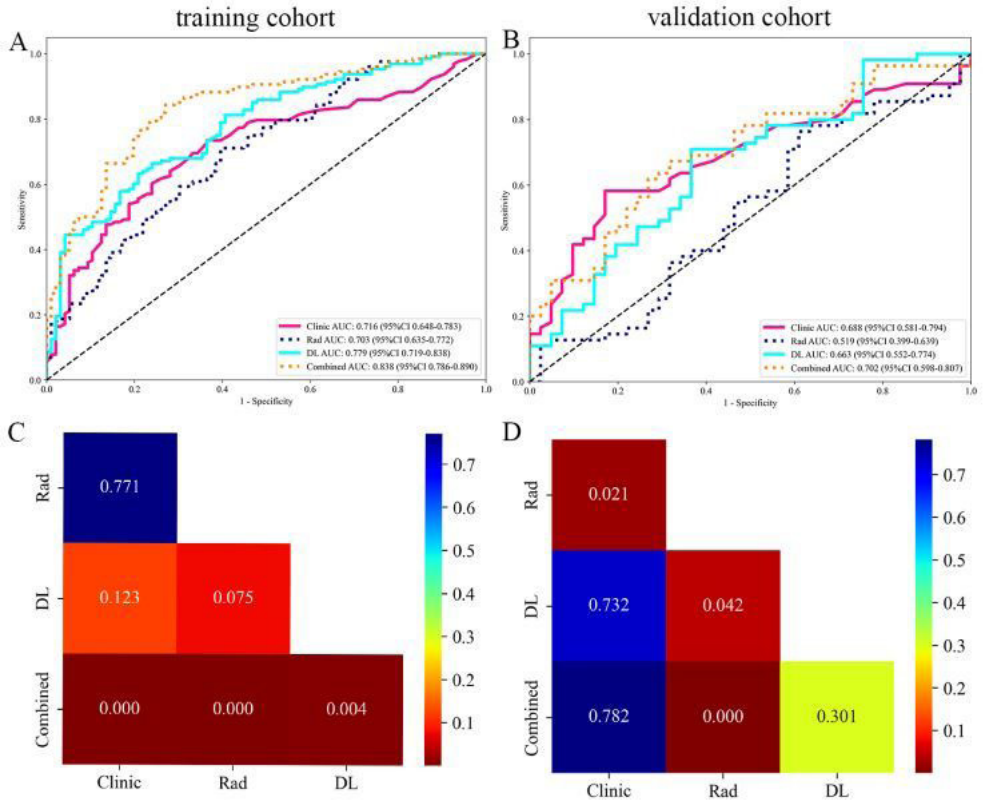

Figure S7 Presents the ROC curves (A: training cohort, B: validation cohort) and DeLong tests (C: training cohort, D: validation cohort) for the assessment of the combined prediction model.

https://dx.doi.org/10.21037/jgo-2025-1-1026